Facile synthesis of Rh/Ti3+-TiO2 nanocomposites and its photodisinfection properties on *Staphylococcus aureus* under visible-NIR excitation

Jingtao Zhang
School of Food and Bioengineering, Zhengzhou University of Light Industry
Shurui Liu
Zhengzhou University of Light Industry
Qinwen Wang
Zhengzhou University of light industry
Jing Yao
Zhengzhou University of Light Industry
Yin Liu
Zhengzhou University of Light Industry
Bingkun Liu
Zhengzhou University of Light Industry
jun xiao (jxiao14b@imr.ac.cn)
Institute of Metal Research, Chinese Academy of Sciences
Hengzhen Shi
Zhengzhou University of Light Industry

Research Article

Keywords: Rh/Ti3+-TiO2, Near-infrared light, Nanocomposites, Self-doped, Antibacterial activity

Posted Date: May 3rd, 2020

DOI: https://doi.org/10.21203/rs.3.rs-25790/v1

Version of Record: A version of this preprint was published at Materials Letters on October 1st, 2020. See the published version at https://doi.org/10.1016/j.matlet.2020.128257.

Abstract

In this study, we synthesized a series of rhodium-modified and Ti^{3+} self-doped TiO_2 (Rh/Ti^{3+}-TiO_2) nanocomposites via the one-pot method. We prepared samples of Rh/Ti^{3+}-TiO_2, which were analyzed using X-ray diffraction (XRD), transmission electron microscopy (TEM), X-ray photoelectron spectroscopy (XPS), Electron Spin Resonance (ESR), and Uv-vis-NIR analysis. We found that the ability of TiO_2 to absorb near-infrared and visible light was significantly improved by the Rh/Ti^{3+}-TiO_2 nanocomposites, due to Ti^{3+} doping as well as modification of Rh. The disinfection properties of these materials were tested using *Staphylococcus aureus* under visible light and NIR light excitations. The synthesized photocatalyst was found to exhibit significantly enhanced photocatalytic inactivation of *S. aureus* under both visible and NIR light irradiation, as compared to pure TiO_2. This was particularly true with respect to the 5% Rh/Ti^{3+}-TiO_2 sample. Our results suggest that the Rh/Ti^{3+}-TiO_2 composites could extend the range of optical response range of pure nano TiO_2 materials to the Vis -NIR region.

1. Introduction

Photodisinfection technology based semiconductors has attracted attention of many researchers as a novel potential bacterial inaction technology in food safety area [1]. Among various studied, TiO_2 was one of the most attractive photocatalyst owing to its properties of high photocatalytic efficiency, high chemical and physical stability, and low cost [2–5]. Previous reports have demonstrated that the TiO_2 photocatalyst can be used for food microorganism disinfection under UV or visible light irradiation [6–9]. Jing and Hung reported that the *Escherichia coli* O157: H7 cell can be inactivated with TiO_2 nanoparticle embedded cellulose acetate films under UV-A light illumination [1]. Muranyi et al. found that the *Kocuria rhizophil* could be reduced 3.3 orders of magnitude on titanium dioxide coated glass slide after 4 h of UV-A light exposure [8]. Xu et al. studied the antibacterial effect of the graphene oxide and chitosan biopolymer loaded TiO_2, and found that the synthesized nanocomposites exhibited high antibacterial activity against *Aspergillus niger* and *Bacillus subtilis* [9]. The photocatalytic antimicrobial performance of a TiO_2 nanocomposite with low-density polyethylene (LDPE) film and its fresh-keeping test for fresh pear were studied by Li et al [10].

However, the low quantum yields and poor efficiency of visible-light use are the two primary challenges for practical applications of pristine TiO_2 [11,12]. A number of methods have been used to overcome these challenges, such as doping with metal or non-metal elements, grouping with other semiconductors, and grouping with plasmonic metal [2,13,14]. Recently, studies on Ti^{3+} self-doped TiO_2 have been carried out due to the ability of this process to overcome the above disadvantages [15–17]. The addition of oxygen vacancies (Ov) or Ti^{3+} to the altered TiO_2 grid greatly improves the photocatalytic ability within the band of visible light [18,19]. Ti^{3+}, when self-doped, also increases the efficiency of separation of the photogenerated charge carriers [20]. The Rh^{3+}-modified TiO_2 exhibited much higher photoactivity than TiO_2 modified by either Cu^{2+} or Fe^{3+} [21].

In this study, we synthesized rhodium-modified and Ti^{3+} self-doped TiO_2 (Rh/Ti^{3+}-TiO_2) nanocomposites using a facile, solvothermal method. In the Vis-NIR area, we found a significantly rate of absorption in the synthesized Rh/Ti^{3+}-TiO_2 nanocomposite samples after analyzing the structure of their crystals using TEM, XRD, and ESR methods. We also confirmed the Ti^{3+} by XPS and ESR analysis. Antibacterial activity was tested using foodborne pathogenic bacteria of *Staphylococcus aureus* under both visible light and near-infrared light irradiation. Our disinfection results demonstrated that *S. aureus* could be disinfected via illumination with Vis-NIR light in the Rh/Ti^{3+}-TiO_2 nanocomposite.

2. Methods

Reagents

$TiCl_4$ (99.5%), $RhCl_3{\cdot}3H_2O$, (38.5–42.5%), and NaOH (98%), were purchased from Aladdin Industrial Corporation (Shanghai, PR China), absolute ethanol (99.8%) was purchased from Sinopharm. Chemical Reagent Co., Ltd. (Shanghai, PR China), and used without further purification. Nutrient agar was BR grade and purchased from Beijing Aoboxing Biotechnology Co., Ltd. (Beijing, PR China). Deionized water was prepared from a lab ultra-pure water purifier.

Fabrication and characterizations of Rh/Ti^{3+}-TiO_2 Nanocomposite

We synthesized the Rh/Ti^{3+}-TiO_2 samples using a one-pot solvothermal reaction, which is briefly described below. First, we dissolved 6 mmol titanium tetrachloride and 0.06 mmol rhodium chloride hydrate (1% molar ratio of titanium tetrachloride) in 30 mL of ethanol, which resulted in a mixture. Then we added 30 mL of NaOH ethanol solution in order to get a fixed molar ratio of NaOH to $TiCl_4$ and $RhCl_3$ of 4:1 and 3:1, at room temperature. During this process, we observed a precipitate while the reaction occurred, for 30 min under vigorous agitation. Lastly, we placed the mix into a 100 mL Teflon-lined autoclave bottle where it was stored for 4 h at 180 ℃. The mix was then allowed to cool to room temperature. Following the solvothermal reaction, we washed the precipitate three times with distilled water and ethanol, after which they were dried at 80 ℃ for 12 h. After the precipitate dried, it was crushed into a fine powder and marked as 1% Rh/Ti^{3+}-TiO_2. We prepared samples with different Rh molar ratios of 3%, 5%, and 7% Rh according to this method, while the TiO_2 without Rh was also prepared for use as a reference.

We analyzed the structure of the crystal using powder X-ray diffraction (XRD) with Cu Kα radiation on a D8 Advance X-ray Diffractometer (Bruker, Germany). The scan rate was 0.5°/min, while the scan range of 2θ was 20° to 80°. Using a JEM-2100 transmission electron microscope (JEOL, Japan), we examined images from the transmission electron microscopy (TEM) and high-resolution transmission electron microscopy (HRTEM). We analyzed Ti^{3+} using Electron Spin Resonance (ESR) spectroscopy on a JES-FA200 (JEOL, Japan) electron spin resonance instrument at 110 K. We studied traces of Ti, Rh, and O in

the Rh/Ti^{3+}-TiO_2 sample via X-ray photoelectron spectroscopy (XPS), and performed XPS measurements with an ESCALAB250 X-ray photoelectron spectrometer (Thermo Fisher Scientific Inc., MA) with an Al K anode (1,486.6 eV photon energy, 300 W). The optical absorbance was calculated from measurements of diffuse reflectance, which we got from a U-3600 UV-VIS-NIR spectrophotometer (Shimadzu, Japan). $BaSO_4$ was the control.

Cell Culture and Viability Assay

Wild type *Staphylococcus aureus* subsp. Aureus (ATCC 6538) cells were kindly provided by Dr. Juan Du, School of Food and Bioengineering, Zhengzhou University of Light Industry. *S. aureus* cells (1% v/v final) were inoculated into Nutrient agar media (the agar without added for the liquid media). The cells were incubated on a BS-1E rotary shaker (Jintan Xinhang Instrument Factory) under 150 rpm and 37 ^oC for 12 h. After overnight culture, cells were harvested by centrifugation at 6000 rpm for 5 min at room temperature, washed twice with a phosphate buffer solution (PBS, pH 7.0), and suspend with the same volume of the Nutrient agar media in PBS (ca. 10^9 CFU/ml). All solid/liquid materials had been autoclaved for 30 min at 121 ^oC before use.

A fixed concentration of 1 mg photocatalyst/mL *S. aureus* suspension was used in the experiments. 10 mg photocatalyst with 9.9 mL buffer solution was first injected into a sterile 60 mm × 15 mm Petri dish and was dispersed ultrasonically for 10 min. Then, 0.1 mL *S. aureus* suspensions (ca. 10^9 CFU/mL) was added into the Petri dish, so that the initial *S. aureus* concentration used in the photoctalytic disinfection experiments was ca. 10^7 CFU/mL.

A 300 W xenon lamp (HSX-F300, Beijing NBET Technology Co. Ltd., Beijing, China) was used for photocatalytic inactivation experiments, and the light with wavelengths below 400 nm and above 700 nm was blocked by glass filters for the disinfection under visible light. In addition, the light with wavelengths below 800 nm and above 1100 nm was blocked by other glass filters for the disinfection under NIR light. A cooling water circulating device was used for keep the temperature under NIR light irradiation (see schematics S1). The light intensity striking the cells was at ca. 30 mW/cm^2, as measured by a FZ-A optical Radiometer (Photoelectric Instrument Factory of Beijing Normal University, Beijing, China).

At regular time intervals, 0.1 mL of the cell suspensions was withdrawn in sequence. Following the appropriate dilution in PBS buffer solution (pH 7), aliquots of 0.1 mL were spread onto an agar medium plate, and incubated at 37 ^oC for 24 h. Then, the number of viable cells in terms of colony-forming units was counted. The comparison experiments in the dark with the photocatalyst and under light illumination only without photocatalyst were also carried out under otherwise identical. All analyses were conducted in triplicate.

3. Results And Discussion

The XRD patterns of Rh/Ti^{3+}-TiO_2 nanocomposite (Fig. 1) indicate that these TiO_2 samples are in the anatase phase. Figure 2 displays the TEM image of the Rh/Ti^{3+}-TiO_2 nanocomposite. The XRD diffraction peak of Rh is clearly visible in the XRD patterns, while the signal strengthened as the atomic ratio of Rh/Ti increased [22]. Figure 2 displays the TEM image of the Rh/Ti^{3+}-TiO_2 nanocomposite. Figure 2(a) displays nanosized particles with non-uniform shapes, with the average particle size being ~ 5 to 10 nm. Figure 2(b) displays the high-resolution TEM (HRTEM) image. The d-spacing was set at ~ 0.35 nm. This aligns with the (101) plane at TiO_2. A group of lattice planes is easily identified on one nanocrystallite, with d-spacing at ~ 0.22 nm, corresponding to the (111) plane of Rh [23]. These lattice planes are clearly visible, which concurs with the results of our XRD analysis.

Using XPS, we examined both the surface components as well as the chemical valence state of the 5% Rh/Ti^{3+}-TiO_2 nanocomposite (Fig. 3). After analyzing the XPS spectrum we found traces of Ti, Rh, and O (Fig. 3a). The Ti 2p XPS spectra of the Rh/Ti^{3+}-TiO_2 nanocomposite was used to determine binding energies at 464.7, 463.9, 458.7, and 458.1 eV, which align, respectively, with Ti^{4+} $2p_{1/2}$, Ti^{3+} $2p_{1/2}$, Ti^{4+} $2p_{3/2}$, and Ti^{3+} $2p_{3/2}$ [15], (Fig. 3b). ESR is particularly useful for detecting the existence of Ti^{3+}, due to its high sensitivity to species containing unpaired electrons. The presence of Ti^{3+} in the 5% Rh/Ti^{3+}-TiO_2 nanocomposite was also identified using low-temperature ESR. A sharp and steep signal at $g = 1.999$ indicates the existence of Ti^{3+} [24] in the Rh/Ti^{3+}-TiO_2 nanocomposite (Fig. 4). In Fig. 3c, the binding energies of Rh $3d_{3/2}$ at 312.2 eV and Rh $3d_{5/2}$ at 307.5 eV can be attributed to the Rh^0 [23] valence states (Fig. 2c). The weak peak binding energies of Rh $3d_{3/2}$ at 314.0 eV and Rh$3d_{5/2}$ at 309.0 are attributed to the Rh^{3+} valence states. There are a number of factors that influence the incidence of Rh^{3+}: partial oxidization during treatment, high surface activity, and a small particle size. The binding energy of 530.0 eV can be attributed to the O lattice of TiO_2, while the peak at 532.0 eV is due to the O lattice of $Ti^{3+,}$ or chemisorbed hydroxyl groups (Fig. 3d).

Figure 5 shows the light absorbance of Rh/Ti^{3+}-TiO_2 nanocomposite. Pure TiO_2 powder (without adding Rh) was also tested as a control. The Rh/Ti^{3+}-TiO_2 nanocomposite showed a clear shift of absorbance in the visible and NIR light range (1100 nm > λ > 400 nm). We also observed that as the atomic ratio of Rh increased, the visible-NIR light absorbance capacity of the Rh/Ti^{3+}-TiO_2 nanocomposite was also increased. The photographs in Fig. 5 are digital photos of the synthesized TiO_2 and Rh/Ti^{3+}-TiO_2 nanocomposite materials. We observed the darkest color of the 7% Rh/Ti^{3+}-TiO_2 nanocomposite, which coincides with the absorbance spectrum of visible light.

Figure 6a and 6b demonstrate the survival ratio of *S. aureus* when treated with Rh/Ti^{3+}-TiO_2 nanocomposites, with different levels of Rh under visible and NIR light illumination (λ = 400–700 nm and λ = 800–1100 nm) when compared to *S. aureus* treated under different conditions (such as visible light or NIR light illumination only, TiO_2 nanoparticles under visible light illumination, and 5% Rh/Ti^{3+}-TiO_2 nanocomposite in the dark). The survival rate of *S. aureus* was 26.3% under visible light and 68.2% under

NIR light, which may be induced by photodamage of the cell. When treated with TiO_2 nanoparticles for 4 h, the survival ratio of *S. aureus* was approximately 20% under visible light and 62.9% under NIR light. Therefore, the TiO_2 nanoparticles demonstrated lower activity for *S. aureus*. Rh/Ti^{3+}-TiO_2 nanocomposites, however, demonstrated an increased ability for photocatalytic disinfection of *S. aureus* under both visible light and NIR light. After 4 h of treatment with 1%, 3%, 5%, and 7% Rh/Ti^{3+}-TiO_2 nanocomposites, the survival ratio of *S. aureus* was approximately 4.7%, 0.56%, 0.0049%, and 0.056%, respectively. An Rh content of 5% displayed the strongest disinfection rate, while the lower disinfection rate of the 7% Rh/Ti^{3+}-TiO_2 nanocomposite could be due to the increased amount of Rh. Without visible light illumination, the survival ratio of *S. aureus* remained constant at 50% after 4 h of treatment with 5% Rh/Ti^{3+}-TiO_2 nanocomposite, which could be explained by mental rhodium nanoparticles accepting the electron of the cell membrane. In Fig. 6b and Figure S1, the survival ratio of *S. aureus* was approximately 6.3% under treatment with the 5% Rh/Ti^{3+}-TiO_2 nanocomposite and NIR light illumination.

4. Conclusions

In conclusion, we successfully synthesized a metallic, rhodium-modified, and Ti^{3+} self-doped TiO_2 nanocomposite photocatalyst using a facile solvothermal method. Our results confirmed that the Ti^{3+} ion and metallic rhodium were both present in the synthesized sample. This indicates that, when illuminated with both visible and NIR light, the synthesized nanocomposite demonstrates enhanced antibacterial activity as compared to pure TiO_2 nanoparticles.

Declarations

Acknowledgments

We are grateful for the National Natural Science Foundation of China (No. 21571160), the National Natural Science Foundation of China-Henan Talents Fostering Joint Funds (No. U1504311), and the Key Research Projects of the Science and Technology Department of Henan Province (No. 182102210153 and 182102210619) for funding.

References

[1] J. Xie, Y.C. Hung, Food Control 106 (2019).

[2] A. Meng, L. Zhang, B. Cheng, J. Yu, Adv. Mater. 31 (2019) 1–31.

[3] Y. Zheng, B. Liu, P. Cao, H. Huang, J. Zhang, G. Zhou, J. Mater. Sci. Technol. 35 (2019) 667–673.

[4] H. Wei, E.F. Rodriguez, A.F. Hollenkamp, A.I. Bhatt, D. Chen, R.A. Caruso, Adv. Funct. Mater. 27 (2017) 1–9.

[5] Y. Wang, M. Zu, X. Zhou, H. Lin, F. Peng, S. Zhang, Chem. Eng. J. 381 (2020) 122605.

[6] Z. Zhu, H. Cai, D.W. Sun, Trends Food Sci. Technol. 75 (2018) 23–35.

[7] A. Jain, S. Ranjan, N. Dasgupta, C. Ramalingam, Crit. Rev. Food Sci. Nutr. 58 (2018) 297–317

[8] P. Muranyi, C. Schraml, J. Wunderlich, J. Appl. Microbiol. 108 (2010) 1966–1973.

[9] W. Xu, W. Xie, X. Huang, X. Chen, N. Huang, X. Wang, J. Liu, Food Chem. 221 (2017) 267–277.

[10] H. Bodaghi, Y. Mostofi, A. Oromiehie, Z. Zamani, B. Ghanbarzadeh, C. Costa, A. Conte, M.A. Del Nobile, LWT - Food Sci. Technol. 50 (2013) 702–706.

[11] M. Ye, J. Gong, Y. Lai, C. Lin, Z. Lin, J. Am. Chem. Soc. 134 (2012) 15720–15723.

[12] H. Hu, Y. Lin, Y.H. Hu, Chem. Eng. J. 375 (2019) 122029.

[13] Q. Guo, C. Zhou, Z. Ma, X. Yang, Adv. Mater. 1901997 (2019) 1–26.

[14] S.G. Kumar, K.S.R.K. Rao, Appl. Surf. Sci. 391 (2017) 124–148.

[15] D. Cheng, Y. Li, L. Yang, S. Luo, L. Yang, X. Luo, Y. Luo, T. Li, J. Gao, D.D. Dionysiou, J. Hazard. Mater. 378 (2019) 120752.

[16] Y. Song, B. Li, Y. Shi, Q. Wang, R. Jin, B. Huang, Y. Dai, S. Gao, Mater. Lett. 252 (2019) 134–137.

[17] W. Fang, M. Xing, J. Zhang, Appl. Catal. B Environ. 160–161 (2014) 240–246.

[18] X. Chen, L. Liu, P.Y. Yu, S.S. Mao, Science (80-.). 331 (2011) 746–750.

[19] K. Li, S. Gao, Q. Wang, H. Xu, Z. Wang, B. Huang, Y. Dai, J. Lu, ACS Appl. Mater. Interfaces 7 (2015) 9023–9030.

[20] F. Zuo, K. Bozhilov, R.J. Dillon, L. Wang, P. Smith, X. Zhao, C. Bardeen, P. Feng, Angew. Chemie Int. Ed. 51 (2012) 6223–6226.

[21] S. Kitano, N. Murakami, T. Ohno, Y. Mitani, Y. Nosaka, H. Asakura, K. Teramura, T. Tanaka, H. Tada, K. Hashimoto, H. Kominami, J. Phys. Chem. C 117 (2013) 11008–11016.

[22] M. Sheikhzadeh, S. Hejazi, S. Mohajernia, O. Tomanec, M. Mokhtar, A. Alshehri, S. Sanjabi, R. Zboril, P. Schmuki, ChemCatChem (2019) 1–6.

[23] S. Bac, Z. Say, Y. Kocak, K.E. Ercan, M. Harfouche, E. Ozensoy, A.K. Avci, Appl. Catal. B Environ. 256 (2019) 117808.

[24] J. Huo, Y. Hu, H. Jiang, C. Li, Nanoscale 6 (2014) 9078–9084.

Figures

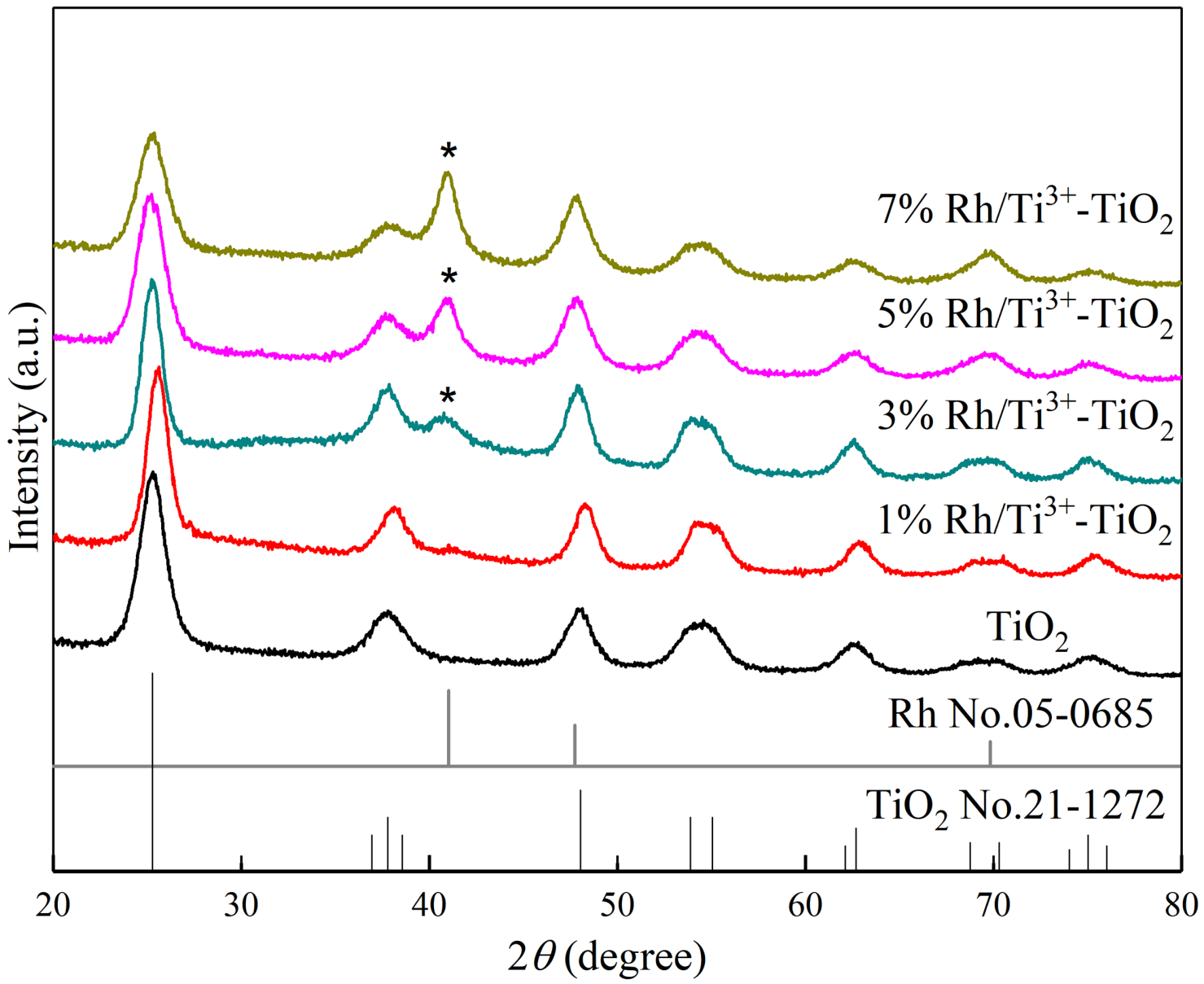

Figure 1

X-ray diffraction patterns of TiO2 nanoparticles and Rh/Ti3+-TiO2 nanocomposite.

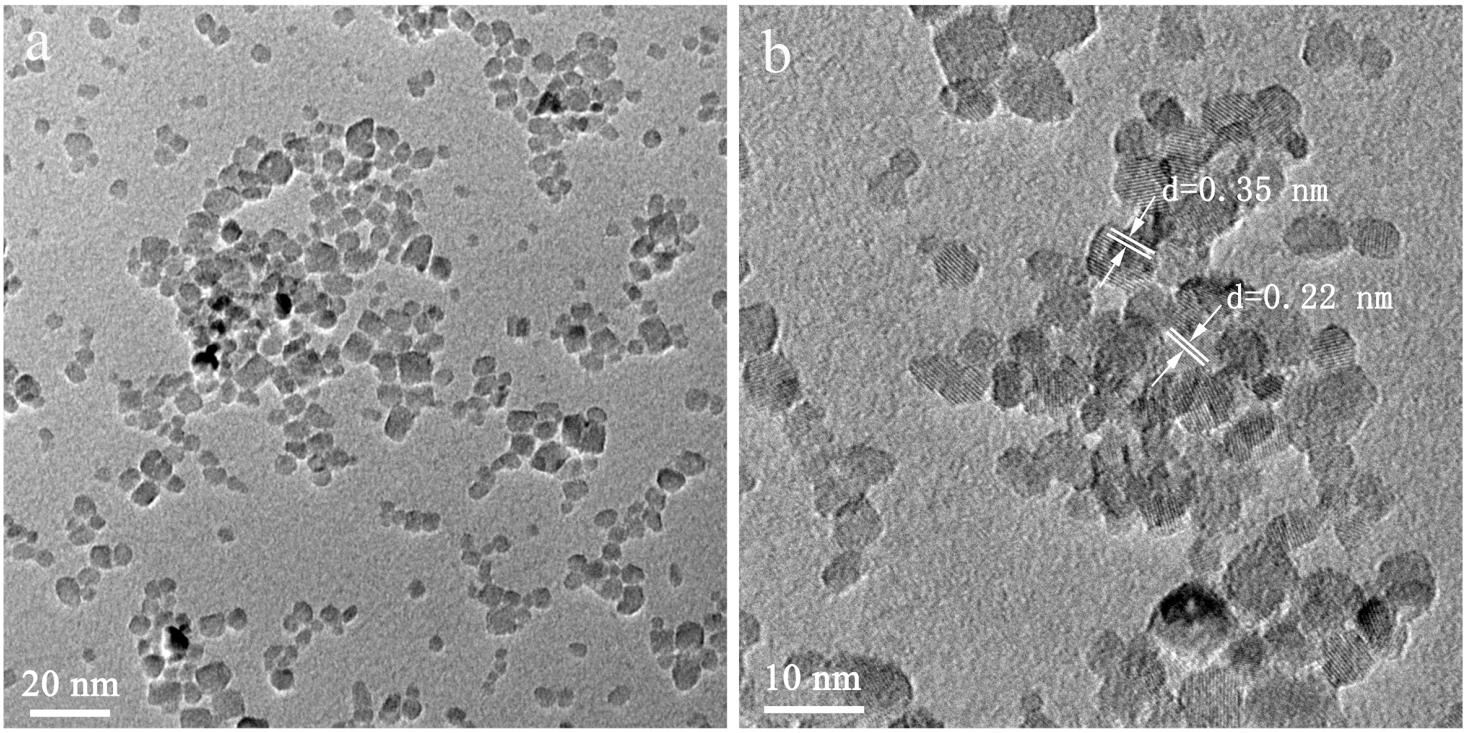

Figure 2

(a) Transmission electron microscopy image of 5% Rh/Ti3+-TiO2 nanocomposite. (b) High Resolution Transmission electron microscopy image of 5% Rh/Ti3+-TiO2 nanocomposite.

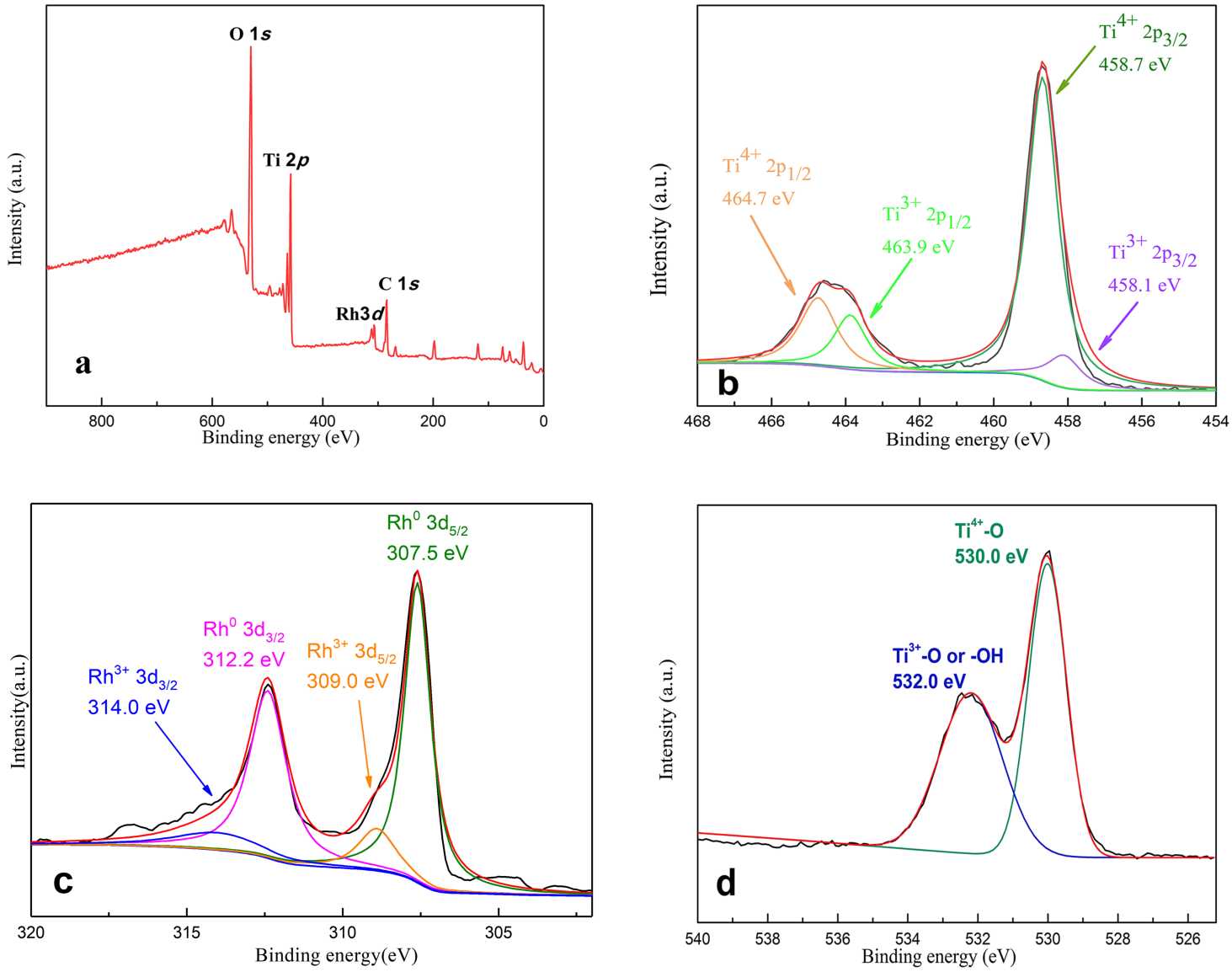

Figure 3

(a) Representative XPS survey spectrum of the 5% Rh/Ti3+-TiO2 nanocomposite. (b) High-resolution Ti 2p XPS spectrum. (c) High-resolution Rh 3d XPS spectrum. (d) High-resolution O 1s XPS spectrum

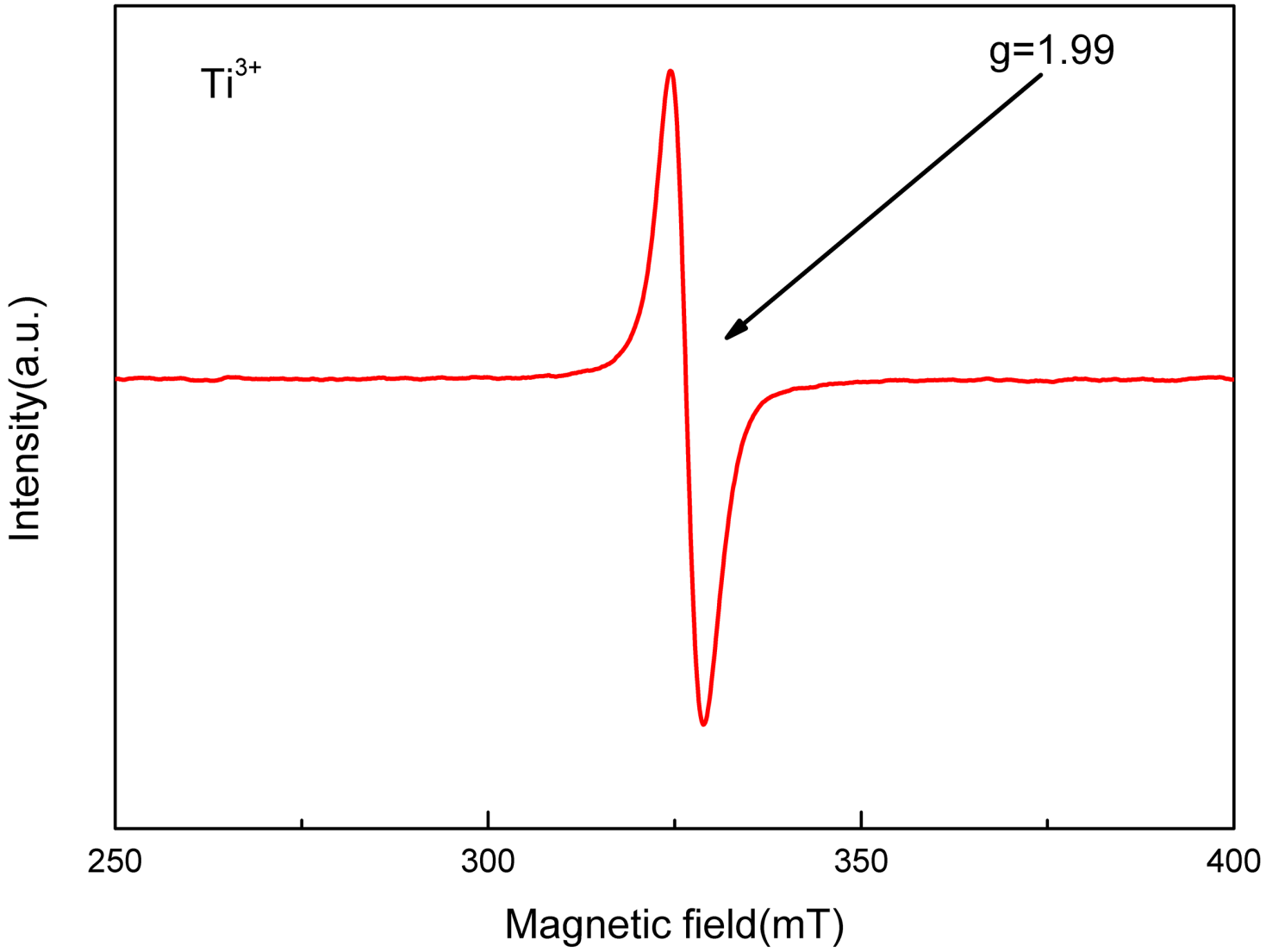

Figure 4

ESR spectra of the Rh/Ti3+-TiO2 nanocomposite.

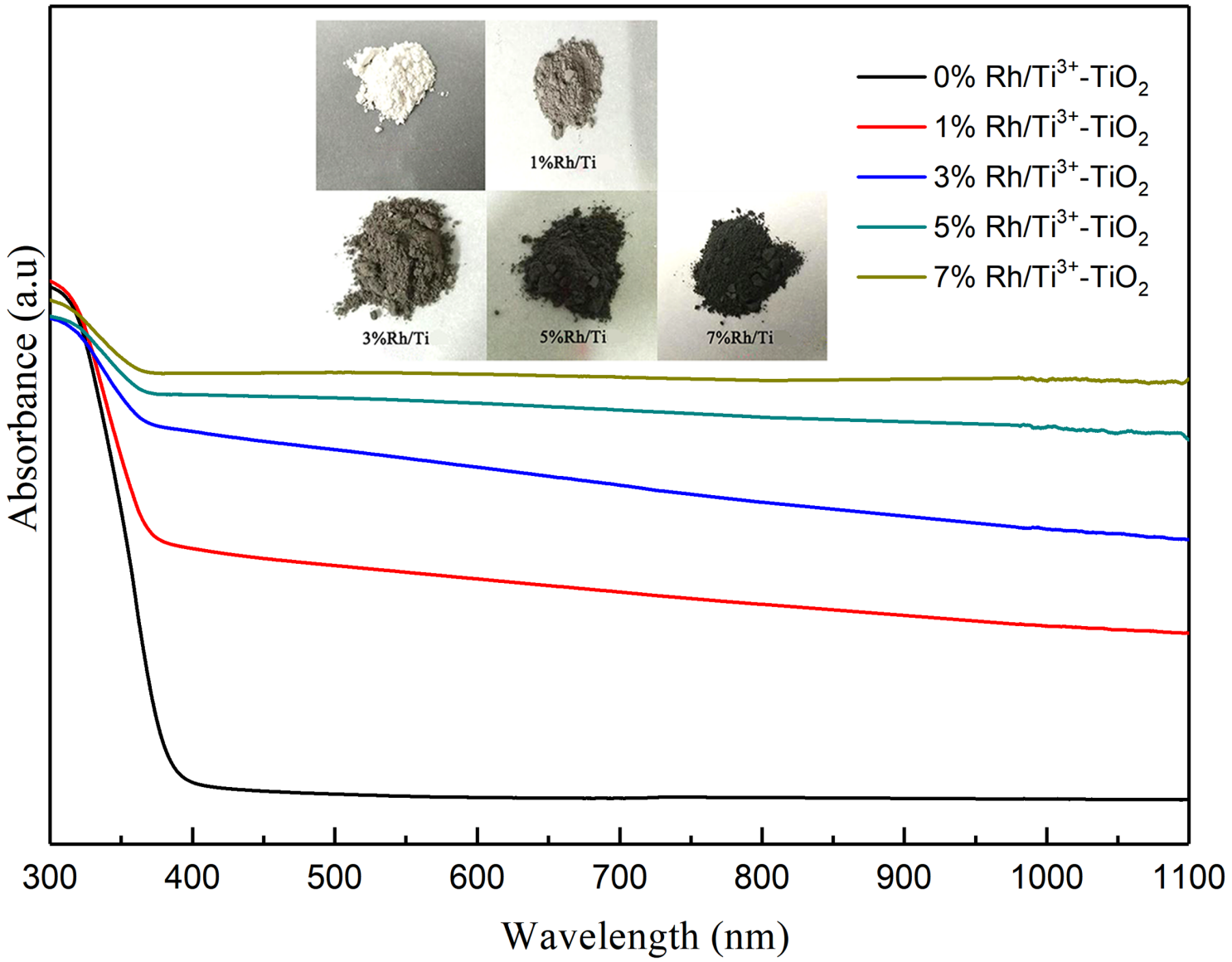

Figure 5

Optical absorbance of Rh/Ti3+-TiO2 nanocomposite, compared with that of TiO2 nanoparticle. The inset pictures were the color of the synthesized Rh/Ti3+-TiO2 nanocomposite.

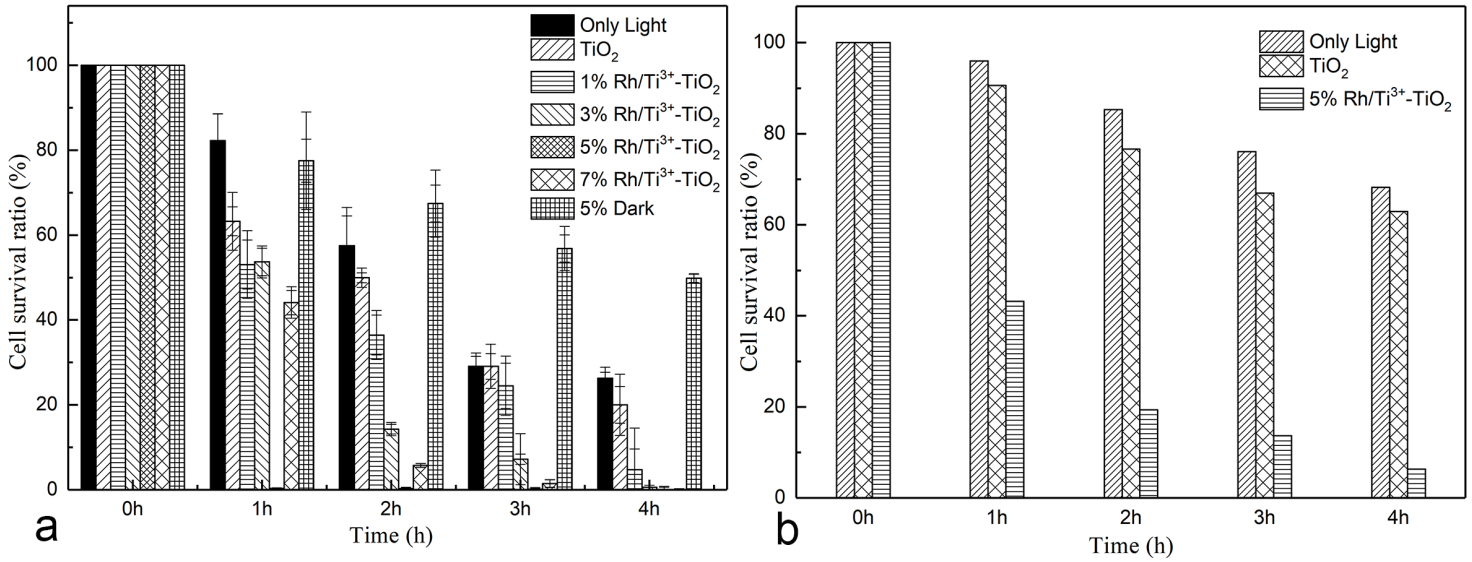

Figure 6

Survival ratio of S. aureus versus various treatments: (a) under visible light illumination without photocatalyst, under visible light illumination (400–700 nm) with TiO2 nanoparticles, in the dark with 5% Rh/Ti3+-TiO2 nanocomposite, and under visible light illumination with 1%, 3%, 5% and 7% Rh/Ti3+-TiO2 nanocomposite; (b) under NIR illumination without photocatalyst, under NIR illumination (800–1100 nm) with TiO2 nanoparticles, and under NIR illumination with 5% Rh/Ti3+-TiO2 nanocomposite. The S. aureus suspension had an initial concentration at ca.107 CFU/mL. The data shown were the average values from three experiments.

Supplementary Files

This is a list of supplementary files associated with this preprint. Click to download.

- FigS.tif
- SchematicsS1.tif
- SupplementaryInformation.docx
- FigS.tif
- SupplementaryInformation.docx
- SchematicsS1.tif